# Modeling and Analysis of 4-Step 3-D Cartesian Braided Composites

Soheil Mohajerjasbi
Boeing Defense & Space Group
Helicopters Division
Philadelphia, Pennsylvania

## ABSTRACT

The fiber architecture of the preform produced in a 4-Step (1x1) 3-D Cartesian braiding process is investigated based on a study of the movement of the fiber carriers on the machine bed. Distinctly different fiber architectures are identified for the interior, boundary, and corner regions of the preform and the composite. Since different fiber architectures will result in different deformation properties, the effective deformation behavior of the composite is expected to be the result of contributions from these different stiffness properties.

In contrast with these findings, some of the the present analytical models consider a "unit cell" as a repeat unit for the braided composite, and attempt to model the mechanical behavior of the composite from the properties of this unit cell. This unit cell is in the form of a parallelpiped with yarns connecting between the opposite corners along the body diagonals.

In this paper, a finite element based method is proposed for modeling the structure of the 3-D braided composite, and determining the elastic constants and coefficients of thermal expansion. MSC/NASTRAN is used in modeling the thermoelastic properties of the composite. Estimates of elastic constants and coefficients of thermal expansion are developed as a function of "interior braiding angle".

Among advantages of this technique are simplicity, and the ability to model and study the response of complex shapes subject to complex loads applied at the boundary.

## INTRODUCTION

The engineering applications of three-dimensional fabrics for composites date back to the late 1960's, responding to the needs in the emerging aerospace industry for parts and structures capable of withstanding multidirectional mechanical and thermal stresses. The 4-Step 3-D braiding process is one of a few processes that produce such a three-dimensional fabric, called a "preform". Each of these different processes produce a preform with a different fiber architecture.

The principal feature of 3-D braided preforms that make them desirable for reinforcing composites is the ability to form a wide range of complex

geometric shapes [1]. Braids can not be made into wide sheets, but can form more complex structures than materials made by any other textile process. Other advantages of this class of composites include delamination resistance, and good energy absorbing capability [2,3,4]. The three-dimensionally integrated nature of these preforms is reported to result in superior damage tolerance.

The basic braiding motion includes the alternate X and Y displacement of yarn carriers on the machine bed followed by a compacting motion applied to the preform. In addition to bias-oriented yarns, axial or longitudinal yarns oriented at $0^{o}$ to the braiding direction may be added to enhance the axial stiffness of the braided composite.

## 4-STEP (1x1) BRAIDING PROCESS

In 4-step 3-D Cartesian braiding process fiber (yarn) carriers, which are loaded with yarns, are arranged on the machine bed (X-Y plane) in rows and columns to form a shape similar to the preform to be produced. Additional fiber carriers are added to the outside of this array in alternating locations. The end of the yarns are tied to a moveable plate above the braiding machine. This plate is moved away from the machine bed in each machine step to allow formation of more preform. Movement of the fiber carriers on the machine bed in a prescribed manner will produce the braided preform above the machine. A schematic of a typical 4-step 3-D braiding machine is shown in Figure 1. Once the preform is formed, it is removed from the braiding machine. The preform is then placed in a tool, impregnated with matrix material and cured. The process examined here, which is commonly used, is referred to as (1x1) since the fiber carriers move one carrier spacing in the X- and Y-direction in the respective machine steps. In practice, a compacting mechanism on the machine is used to beat up on the preform already made to produce a tight braid. The angle the yarns in the interior of the preform make with the Z-axis, $\gamma$, is defined as "interior braiding angle".The compacting action is important as it influences the interior braiding angle. The original carrier configuration on the machine bed is repeated after every four steps, therefore the name 4-step braiding.

## INTERIOR FIBER ARCHITECTURE

For sake of illustration and examination of the structure of the preform, the movements involved in braiding a square section with only four carriers on each side is shown in Figure 2. The plane of the machine is considered as the X-Y plane, with the Z-axis denoting the braiding axis. The numbers and shadings in this figure have no significance and are only provided for visual aid and identification. The original carrier configuration is shown in Figure 2(a). In the first two machine steps, alternate rows (columns) are moved in opposite directions as shown in Figures 2(b) and 2(c).

In the remaining two steps this horizontal and vertical movement is repeated in reverse. The last two steps are illustrated in Figures 2(d) and 2(e). These movements of the fiber carriers on the machine bed produces the 3-D braided preform above the machine under the moveable plate (x-y plane). By superposition of the yarn structure produced in the first two steps , Figure 2(c), and the yarn structure produced in the last two steps, Figure 2(e), the structure of the 3-D braid formed in four steps may be obtained. With the convention that solid arrows represent the direction of the yarns in the first two steps and the dashed arrows represent the direction of the yarns in the last two steps, and with the understanding that the beginning points of these arrows are raised with respect to their tip, the structure of the preform produced during the 4-steps can be shown in a "compact form" as in Figure 3(a). The boundaries and corners of this "compact form" are shaded differently. The fiber architecture in these areas are discussed in the following section. Any subsequent four machine steps will produce an identical structure. Figure 3(b) shows a schematic view of the yarns in the interior of the braid. The angle of inclination of these yarns with respect to the Z-axis, $\gamma$, is defined as "interior braiding angle". Figure 3(c) shows these interior yarns in a cubical cell, with the size of the yarns reduced to provide visibility into the cell. Figure 3(d) shows these two cells, stacked one on top of the other, in the Z-direction. To summarize, if one idealizes the interior of the braided composite as a cube of matrix material encapsulating the yarns , the fiber architecture in the interior of the preform can be considered as shown in Figure 3(d). For sake of simplification of the modeling approach that will be proposed in the following sections, an idealization is introduced here. Instead of idealizing these yarns as encapsulated inside the cube, they are moved to the sides of the cube, connecting between the opposite corners, as shown in Figure 3(e). It is evident that the "interior braiding angle" , $\gamma$, is preserved.

## BOUNDARY & CORNER FIBER ARCHITECTURE

Figures 4(a) and 4(b) show the carrier movements forming the interior, the boundaries and the corners of the preform. A comparison of Figures 4(a) and 4(b) shows that the carrier movements that result in formation of the boundaries and corners of the preform are distinctly different from the carrier movements that produce the interior of the braid. The reason for this is the fact that the carriers in the top and bottom rows do not participate in any row motion and the carriers in the left-most and right-most columns do not participate in any column motion. Figure 5(a) is a representation of the interior structure of the braided composite next to the boundary. It is seen that the interior is represented by alternating the two types of interior cells introduced before. Figure 5(b) shows this interior structure as a consequence of the idealization introduced earlier. Figure 5(c) shows an approximation of the fiber architecture at the boundary. As a consequence of the idealization introduced for the interior cells, the idealized fiber architecture in the

boundary would be as shown in Figure 5(d). Examination of the idealized structure of the boundary shows that the boundary could be visualized as being made up of two similar, but not identical, cells that repeat themselves in every four machine step.

Figure 5(e) shows an approximation to the fiber architecture in the corner of the preform. As a consequence of the idealization introduced for the interior cells before, the idealized fiber architecture in the corner would be as shown in Figure 5(f). Examination of the idealized structure of the corner shows that the corner could be visualized as being made up of two different cells that repeat themselves in every four machine step.

Since fiber architecture in the interior, the boundary and corner of the preform are different, and different fiber architectures imply different stiffness properties, the proportion of interior, boundary, and corner in a section is expected to influence the deformation behavior of the composite. This may be interpreted as a "Scale Effect". When a large section is considered, the proportion of interior cells is bigger and the properties of the interior cells are expected to dominate the composite properties, while when a thin section is considered one would expect the properties of the boundary cells to dominate the composite properties. It is important to note that the manner of approximation of the fiber architecture at the boundary and the corner will influence the analytical predictions for the average engineering constants of the composite.

## MODELING

The traditional approach in mechanics modeling of composites reinforced by 3-D braided preform has been based on a "unit cell". This unit cell is shaped like a cube with fibers (yarns) running along the body diagonals connecting opposite corners. Starting with this unit cell different approximations and formulations had been proposed for predicting the deformation behavior of the 3-D braided composites.

In the approach proposed in this paper, a finite element based method is pursued in modeling the structure of the 3-D Cartesian braided composite.

This modeling approach is based on the following assumptions and approximation. Consider a composite of volume V, comprised of a volume $V_m$ of matrix and a yarn segment with volume $V_f$. Define a 1-2-3 axis system with the 1-axis directed along the axis of the yarn, and axes 2 and 3 defining a plane perpendicular to the yarn. It is assumed that the composite properties for the yarn segment embedded in the matrix may be found by a rule of mixture as follows, [5]:

$$E_{11} = v_f E_{f_{11}} + v_m E_m = \frac{V_f}{V} E_{f_{11}} + \frac{V_m}{V} E_m$$

$$E_{22} = E_{33} = \frac{E_m}{1 - \sqrt{v_f}\left(1 - \frac{E_m}{E_{f_{22}}}\right)}$$

$$v_{12} = v_f v_f + v_m v_m$$

where the parameters with subscript f and m refer to the fiber and matrix, respectively and $E_{11}$, $E_{22}$, $E_{33}$, and $v_{12}$ define the composite properties. It is noted that this approximation may not account for all the relevant composite properties.

It is proposed that these composite properties may be obtained, with some approximation, by the superposition of two "reinforcing mediums":

1- A "modified matrix" occupying the entire volume V with the following isotropic properties:

$$\bar{\bar{E}}_m = E_{22} \qquad \bar{v}_m = v_{12}$$

2- A "modified yarn" with no transverse stiffness, with the following axial property:

$$\bar{\bar{E}}_f = E_{f_{11}}\left(1 - \frac{\bar{\bar{E}}_m}{E_{f_{11}}}\right)$$

Once these two "reinforcing mediums" are superimposed, with the requirement that the displacements be the same, the stiffness properties in the direction of the axis of the yarn is recovered as follows:

$$V E_{11} = V_f \bar{\bar{E}}_f + V \bar{\bar{E}}_m = V_f E_{f_{11}}\left(1 - \frac{\bar{\bar{E}}_m}{E_{f_{11}}}\right) + V \bar{\bar{E}}_m$$

$$= V_f E_{f_{11}} - V_f \bar{\bar{E}}_m + V \bar{\bar{E}}_m = V_f E_{f_{11}} + V_m \bar{\bar{E}}_m$$

or

$$E_{11} = v_f E_{f_{11}} + v_m \bar{\bar{E}}_m$$

For a typical Graphite/Epoxy composite with a 50% fiber volume fraction the above approximation will overestimate the local axial modulus of the composite by 0.6 Msi. The transverse properties of the composite are only due to contribution from the "modified matrix" with properties as shown above.

Based on the above approximation one may consider the 3-D braided composite as a superposition of a "modified matrix model" and a "modified yarn model", with properties adjusted as shown above, while requiring that the two models have the same u,v, and w displacements at the common nodes.

A schematic view of the finite element model that represents the structure of a repeat unit of the braided composite is shown in Figure 6(a). The model is defined by grids on three planes which correspond to the lower, middle, and the upper planes of this repeat unit. The grids on each plane are defined in different coordinate systems. By moving the coordinate system of the mid-plane and the top plane in the Z-direction, different "interior braiding angles" are simulated. Axial, hexa, and penta elements are used to connect to these grids in the form of the cells introduced earlier. Figures 6(b) through 6(d) show the interior cells, boundary cells, and corner cells used in this finite element model. The "modified yarns" are modeled as axial elements having axial stiffness. The "modified matrix" is modeled as hexa and penta elements with isotropic properties.

In 3-D braided composite, fiber volume fraction is a function of braiding angle. The total length of yarns in the model is found from the length of the yarns in the individual interior, boundary, and corner cells and the number of each type of cell that makes up the preform. Based on the total volume of the model, the total length of yarns in the preform, and the desired fiber volume fraction, the area for these axial elements in the model is calculated.

In order to demonstrate the "Scale Effect" which was introduced in an earlier section, two finite element models are constructed. One with four yarns per side [4x4], and one with eight yarns per side [8x8].

The model is constrained to remove the rigid body motion and different boundary conditions are applied to calculate the different average elastic constants of the braided composite. For example in order to calculate the average Young's modulus in any direction, the nodes on one face of the model are constrained in that direction only, and the nodes on the opposite face are displaced by the amount needed to produce a unit strain in that direction. The SPC-forces on the nodes of the displaced face of the model are summed up and divided by the area of that face of the model to find the average applied stress. Since a unit strain is applied, the calculated average stress is considered to represent the Young's modulus in that direction. In order to calculate the shear moduli of the composite, displacements are applied to the nodes on four faces to produce a unit shear strain. For example to calculate $G_{xy}$ , displacements u and v are imposed on the left, right, front, and back faces as a function of their coordinates (x,y) and with the proper sign to produce a unit shear strain. Summation of SPC-forces in the y-direction on the right face is found and divided by the area of that face to calculate average shear stress. Since a unit shear strain is applied, the calculated average shear stress is considered to represent the shear modulus in that plane. Poisson's ratios are found by calculating the average transverse strain due to a unit

strain in the primary direction. Average strain in a particular direction is found by calculating the difference in the average displacement of the nodes on two opposite faces in that direction and dividing by the distance between the two faces. In order to calculate the thermal expansion properties of the composite the model is only constrained to remove the rigid body motion. Only a 1 degree thermal load is applied to the model, with no other applied load or enforced deformation, and average strains are calculated as stated earlier. Since a unit temperature is applied the resulting average strain in any particular direction is considered to represent the thermal coefficient of expansion in that direction.

## TYPICAL ANALYTICAL RESULTS

In order to demonstrate the predictions of this approach, a typical graphite epoxy system with 50% fiber volume fraction is considered. The typical properties of the graphite and epoxy matrix are as follows:

| | | | |
|---|---|---|---|
| $E_f = 34 \times 10^6$ | psi | $E_m = 0.5 \times 10^6$ | psi |
| $\nu_f = 0.22$ | | $\nu_m = 0.34$ | |
| $\alpha_f = -1.0 \times 10^{-6}$ | in./in. $^oF$ | $\alpha_m = 50 \times 10^{-6}$ | in./in. $^oF$ |

Estimates of elastic constants for the [4x4] and [8x8] model are developed as a function of "interior braiding angle". These predictions are shown in Figures 7(a) through 7(g). The model's predictions are shown for an "interior braiding angle" in the range of $5^o$ to $85^o$. In practice, due to geometric limitations, preforms can not be braided to large braiding angles covered by the predictions. Figures 7(a) through 7(g) show that the proposed "Scale Effect" appears to be more pronounced for certain elastic constants. Also, the predictions of the [8x8] model for the coefficients of thermal expansion are shown in Figures 8(a) and 8(b).

The following is a discussion of the predictions of the model. Figures 7(a) and 7(b) show that the braided composite has the same modulus of elasticity in the x- and y-direction. These figures also show that the transverse modulus of elasticity is not very sensitive to the "interior braiding angle". The transverse properties (i.e. in the x-y plane) appear to be dominated by the matrix properties. Figure 7(c) shows the variation of modulus of elasticity in the direction of axis of braiding, as a function of "interior braiding angle". One can visualize that as the "interior braiding angle" becomes very small the model resembles a unidirectional composite. At small braiding angles (5 degrees) the model predicts a modulus of about $17.2 \times 10^6$ psi. For a unidirectional laminate with 50% fiber volume fraction, rule of mixtures results in a value of $17.25 \times 10^6$ psi. At large braiding angles (85 degrees), the model predicts the modulus of elasticity to be that of the modified matrix, about $1.48 \times 10^6$ psi. Figure 7(d) shows the variation of shear modulus in the

x-y plane with the "interior braiding angle". At small braiding angles, the yarns are directed approximately in the Z-direction and shear modulus of the braided composite in the x-y plane is expected to be dominated by the matrix properties. The model's prediction for shear modulus at small braiding angles (5 degrees) is $4.14 \times 10^5$ psi, which is equal to the modified matrix shear modulus. As the interior braiding angle increases, the axial elements in the interior cells become increasingly closer to the x-y plane, and at $\gamma = 90^o$ the model resembles a +/- $45^o$ laminate. The shear modulus of a +/- $45^o$ laminate with 50% fiber volume fraction may be found from laminate analysis codes to be $4.5 \times 10^6$ psi. The prediction of the model for $G_{xy}$ at $\gamma = 85^o$ is $3.77 \times 10^6$ psi. Figure 7(e) shows the variation of shear modulus in the x-z plane ($G_{xz}$) with "interior braiding angle". At very small braiding angles one would expect this modulus to be dominated by the matrix shear modulus which is $4.14 \times 10^5$ psi. At $\gamma = 5^o$ the model's prediction for $G_{xz}$ is $4.63 \times 10^5$ psi. As the interior braiding angle approaches $\gamma = 90^o$, the model resembles a +/- $45^o$ laminate. The out of plane shear modulus of this laminate is expected to be dominated by the matrix shear modulus. The model's prediction at $\gamma = 85^o$ is $G_{xz} = 4.29 \times 10^5$ psi compared to $4.14 \times 10^5$ psi for the modified matrix. The first index in Poisson's ratio refers to the direction of loading , and the second index refers to the direction of induced strain. Figure 7(f) shows the variation of Poisson's ratio in the x-y plane ($\nu_{xy}$) with the "interior braiding angle". The model predicts that the Poisson's ratio in the x-y plane shows small variation for a broad range of "interior braiding angles" less than $50^o$. Figure 7(g) shows the variation of Poisson's ratio in the x-z plane ($\nu_{zx}$) with the "interior braiding angle". At small braiding angles, where the braided composite resembles a unidirectional composite, one would expect the Poisson's ratio to be dominated by the matrix. At $\gamma = 5^o$ the model predicts a value of 0.30 compared to the Poisson's ratio of the modified matrix of 0.28. As the "interior braiding angle" increases to values close to $\gamma = 90^o$ , the stiffening effect of the yarns in the x-y plane will result in smaller value for $\nu_{zx}$ , about 0.07, as is seen from Figure 7(g).

The same [8x8] finite element model is used to make predictions for expansional strains due to unit temperature rise, which may be considered as coefficients of thermal expansion. The variation of these thermal coefficients of expansion in the x- and z-direction are shown in Figures 8(a) and 8(b), respectively. Ref [6] reports the results of an investigation of the coefficients of thermal expansion for angle-ply laminates made from different material systems. The theoretical derivation and experimental verification for all material systems investigated in Ref [6] show similar trend as Figure 8(b). The dip in the curve in Figure 8(b) appears to be a physical phenomena, independent of the material system used.

## CONCLUSION

The fiber architecture of the preform produced in a 4-Step (1x1) 3-D Cartesian braiding process is investigated based on a study of the movement of the fiber carriers on the machine bed. Distinctly different fiber architectures are identified for the interior, boundary, and corner regions of the preform and the composite.

A finite element based method is proposed for modeling the structure of the 3-D braided composite, and determining the elastic constants and coefficients of thermal expansion.

Elastic constants predicted by the model for small interior braiding angles approach the values of the unidirectional composite, and for large braiding angles (close to $90^{o}$) they approach the elastic constants for a $+/-45^{o}$ laminate.

## ACKNOWLEDGEMENT

The work reported here was supported by The Boeing Defense & Space Group, Helicopters Division. The author wishes to acknowledge, with gratitude, the support of Dr. John Shaw, Deputy Director of Technology and Dr. C. Gunther, Manager of Structures R &D at Helicopters Division. Their constant support and encouragement was very much appreciated.

## REFERENCES


1- F. K. Ko in T. W. Chou and F. K. Ko (Eds.), "Textile Structural Composites", Elsevier Publishers, 1989.

2- R. T. Brown, "Through-The-Thickness Braiding Technology", 30th National SAMPE Symposium, 1985, pp. 1509-1518.

3- W. Li, M. Hammad, and A. El-Shiekh, "Effect of Braided Process on the Damage Tolerance of 3-D Braided Graphite/Epoxy Composites", 34th International SAMPE Symposium, 1989, pp. 2109-2117.

4- F. K. Ko, P. Fang, and H. Chu, "3-D Braided Commingled Carbon Fiber/PEEK Composites", 33rd International SAMPE Symposium, 1988, pp. 899-911.

5- C. C. Chamis, "Simplified Composite Micromechanics Equations for Hygral, Thermal, and Mechanical Properties", SAMPE Quarterly, April 1984, pp. 14-23.

6- J. C. Halpin and N. J. Pagano, "Consequences of Environmentally Induced Dilatation in Solids", AFML-TR-68-395, December 1969.

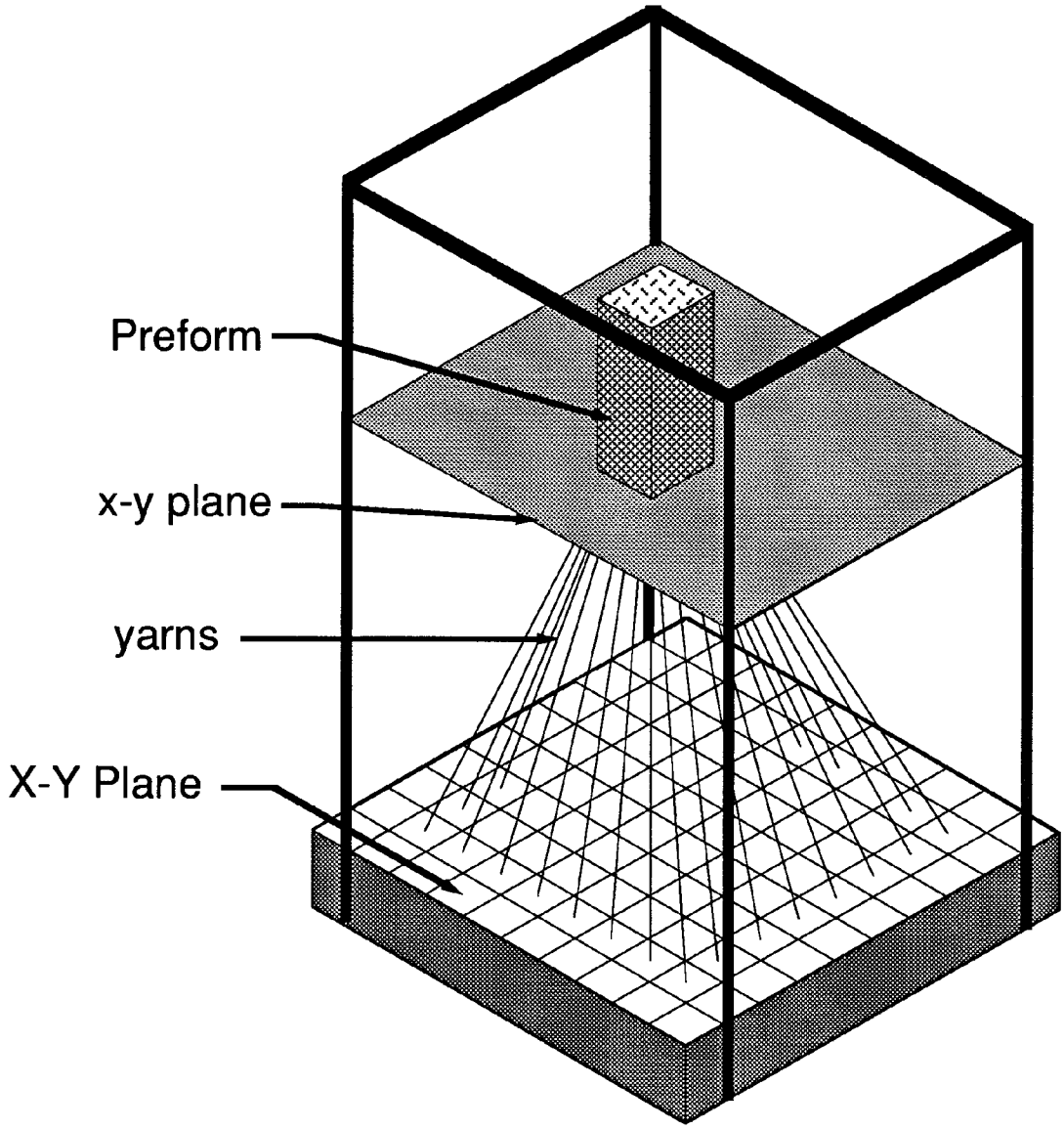


Figure 1- Schematic of a typical 4-step
3-D braiding machine

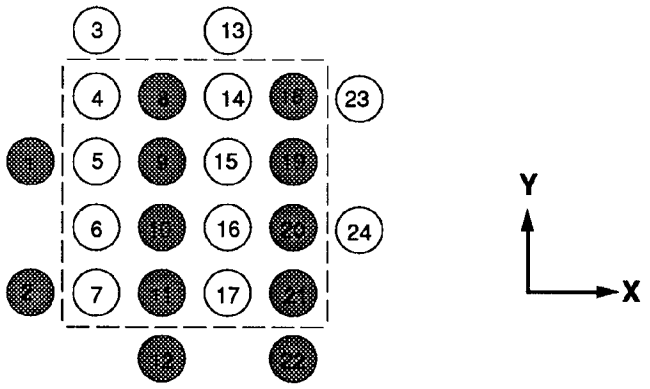


Figure 2(a)- Original carrier configuration - Step 0

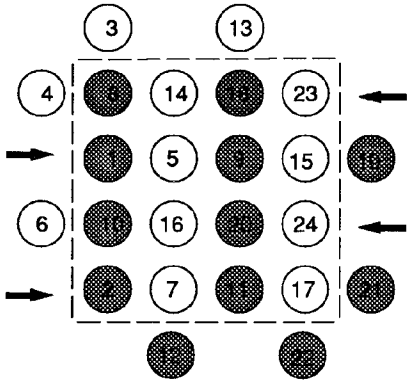

Figure 2(b)- Row movement by one carrier spacing - Step 1

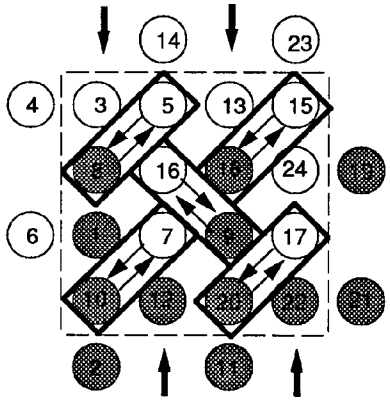

Figure 2(c)- Column movement by one carrier spacing - Step 2

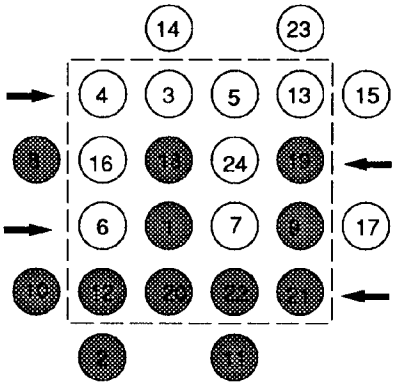

Figure 2(d)- Row movement by one carrier spacing - Step 3

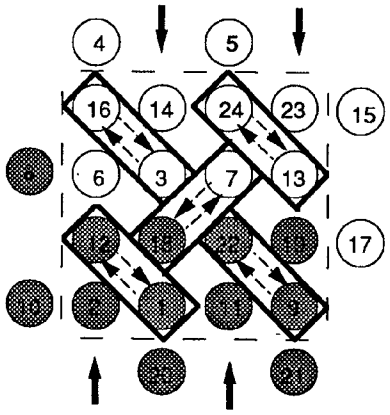

Figure 2(e)- Column movement by one carrier spacing - Step 4

# Figure 2- Machine movements in 4-step process

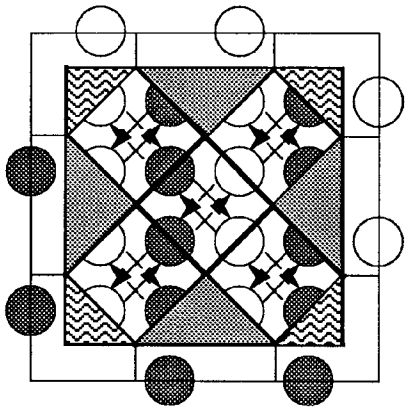

Figure 3(a) - Fiber architecture in the interior of preform

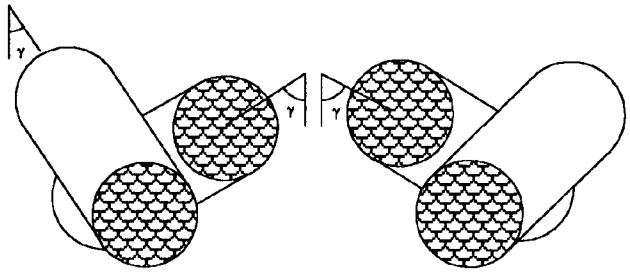

Figure 3(b) - Schematic of yarn formation in the interior of the braid

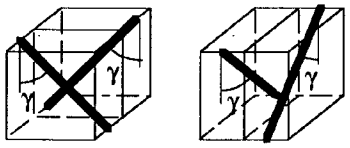

Figure 3(c) - Yarn structure of interior

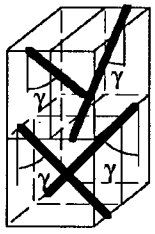

Figure 3(d) - Interior structure along braiding axis

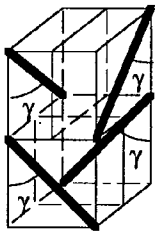

Figure 3(e) - Idealization of Interior structure

Figure 3- Interior structure of braided preform

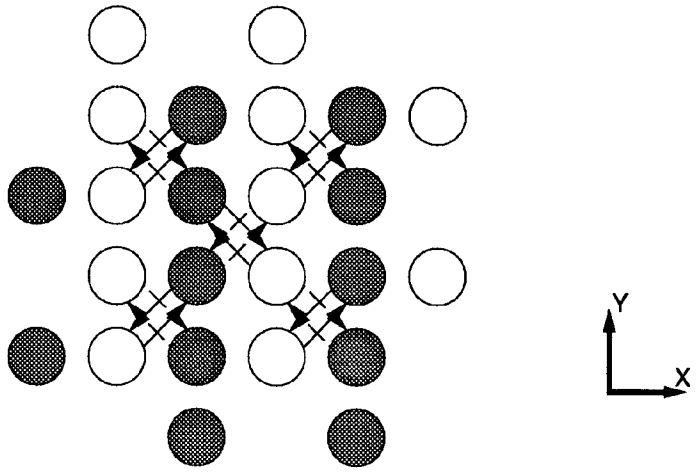


Figure 4(a)- Carrier movements making the interior structure

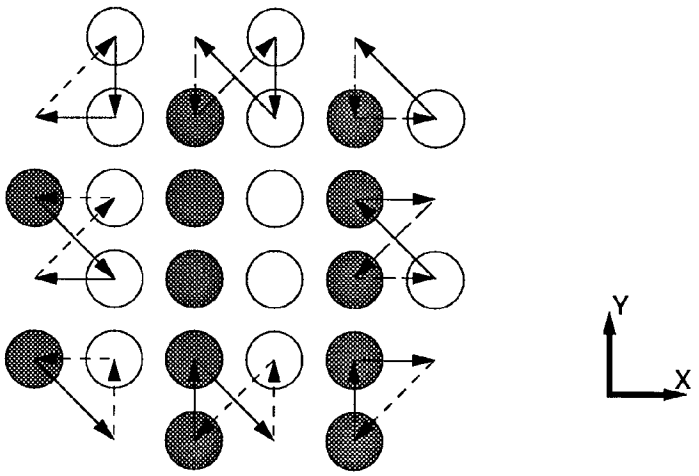


Figure 4(b)- Carrier movements making the boundary and corner of the preform

Figure 4- Carrier movements making the interior, boundaries and corners of the preform

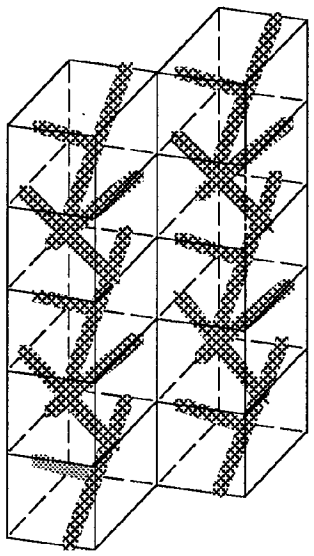

Figure 5(a)- Approximation of fiber architecture in the interior

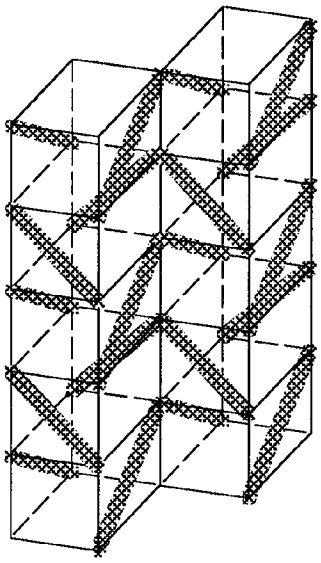

Figure 5(b)- Idealization of fiber architecture in the interior

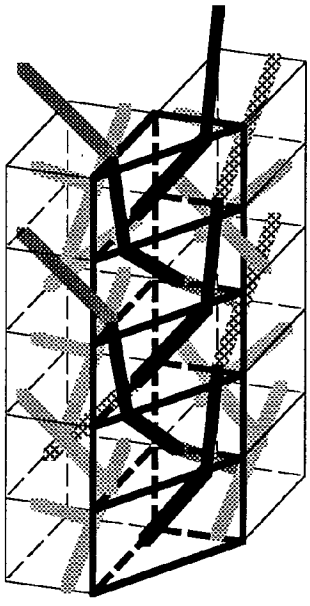

Figure 5(c)- Approximation of fiber architecture at the boundary

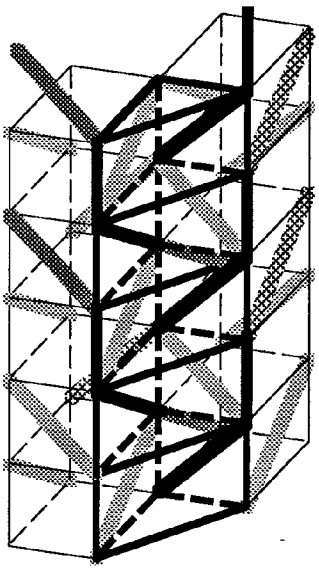

Figure 5(d)- Idealization of fiber architecture at the boundary

Figure 5- Fiber architecture at the interior, boundary, and corner

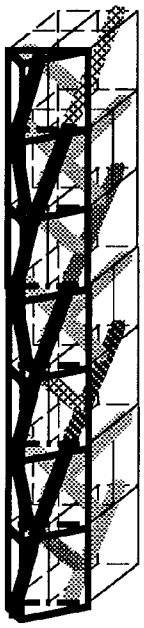

Figure 5(e)- Approximation of fiber architecture at the corner

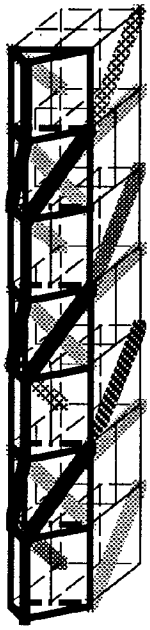

Figure 5(f)- Idealization of fiber architecture at the corner

Figure 5(Continued)- Fiber architecture at the interior, boundary, and corner

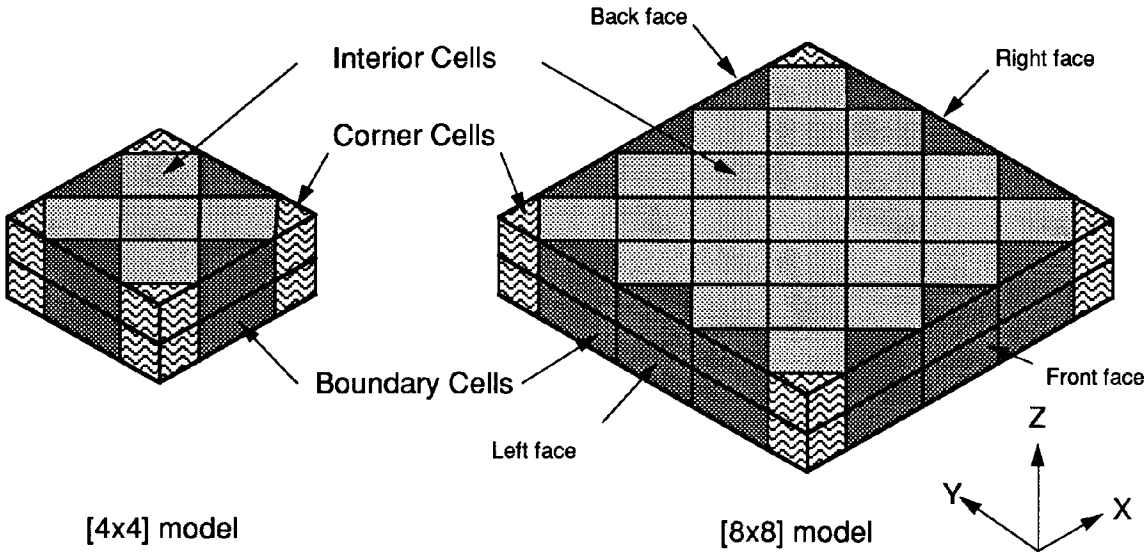


Figure 6(a)- Schematic of the finite element model

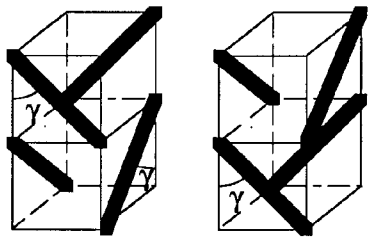

Figure 6(b)- Interior cells

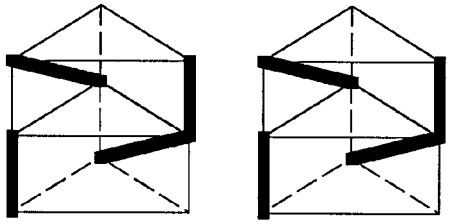

Figure 6(c)- Boundary cells

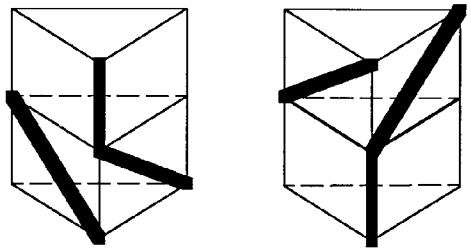

Figure 6(d)- Corner cells

Figure 6- Finite element model of the structure of preform produced during 4-Steps

GR/EPOXY $V_f$ =0.50

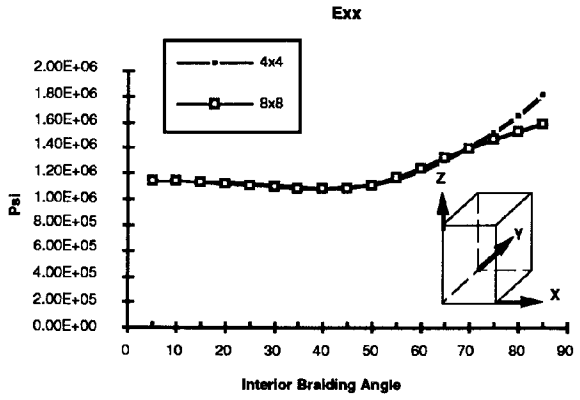


Figure 7(a)- Transverse modulus of elasticity X-Direction

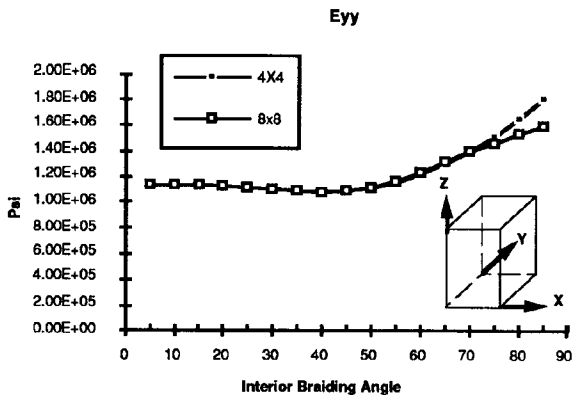


Figure 7(b)- Transverse modulus of elasticity Y-Direction

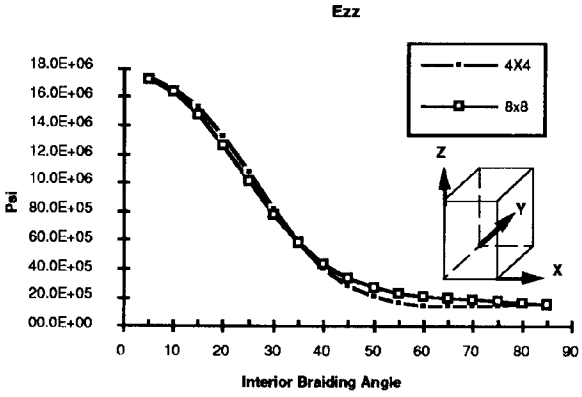


Figure 7(c)- Axial modulus of elasticity Z-Direction

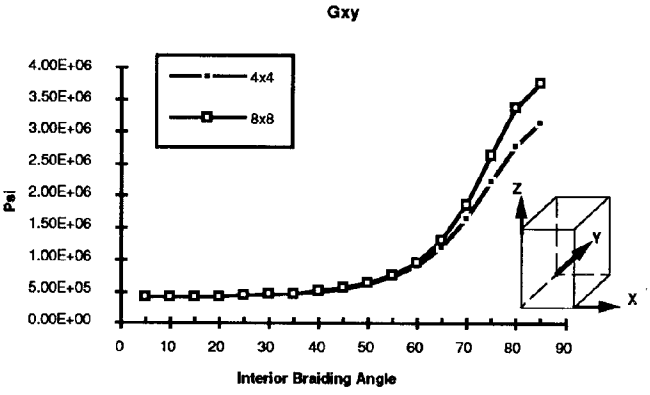


Figure 7(d)- Transverse shear modulus - XY plane

Figure 7- Elastic constants of 3-D braided composite

GR/EPOXY $V_f = 0.50$

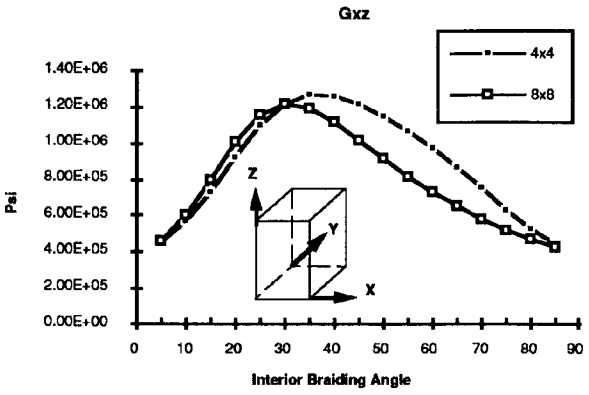


Figure 7(e)- Shear modulus - XZ plane

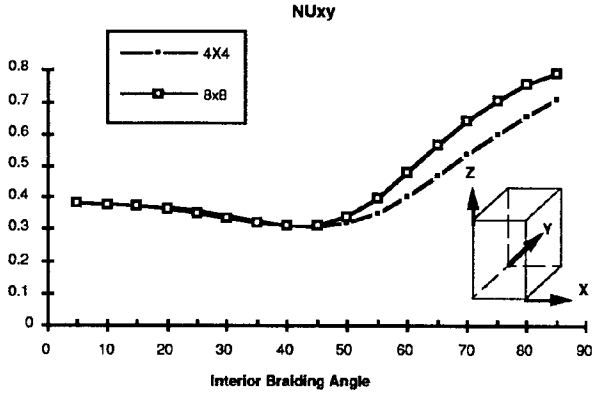


Figure 7(f)- Poisson's ratio - XY plane

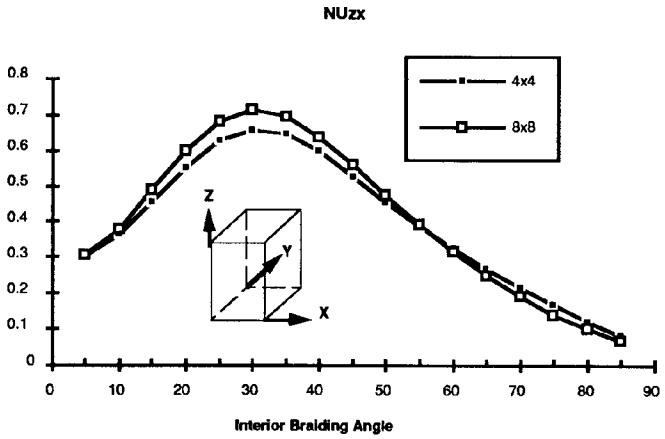


Figure 7(g)- Poisson's ratio - XZ plane

Figure 7(Continued)- Elastic constants of 3-D braided composite

GR/EPOXY $V_f$ =0.50

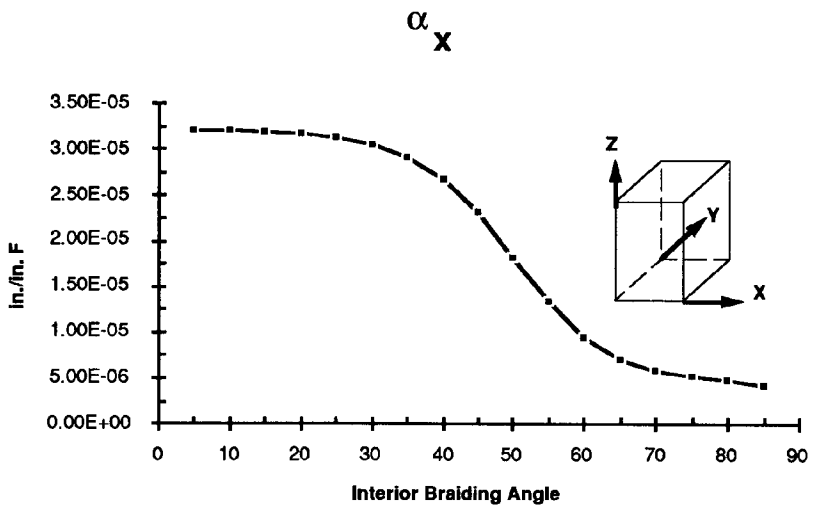


Figure 8(a)- Coefficient of thermal expansion
X-direction

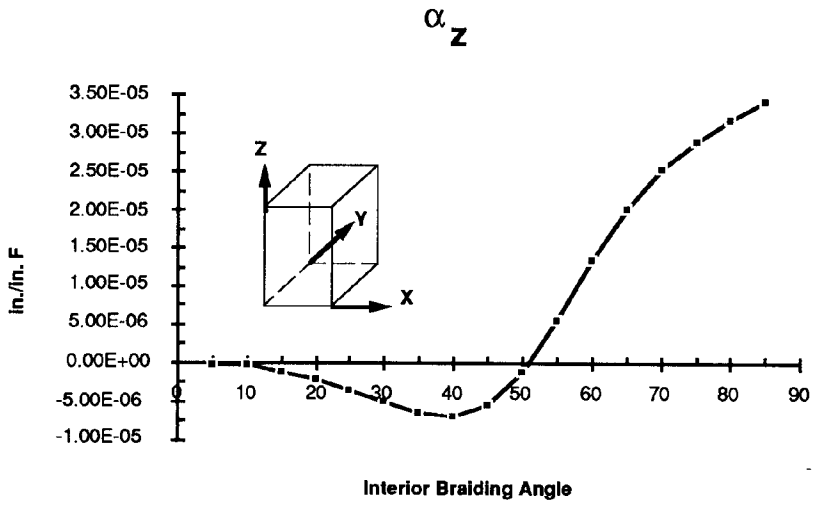


Figure 8(b)- Axial coefficient of thermal expansion
Z-Direction

Figure 8- Coefficients of thermal expansion of 3-D braided composite